# Observation of Many Coherent Oscillations for MeV Protons Transmitted through Stacking Faults

M. B. H. Breese, E. J. Teo, M. A. Rana, L. Huang, J. A. van Kan, and F. Watt

*Physics Department, National University of Singapore, 10 Lower Kent Ridge Road, Singapore 119260*

P. J. C. King

*Rutherford Appleton Laboratories, Chilton OX11 OQX, United Kingdom*
(Received 7 May 2003; published 29 January 2004)

High spatial resolution, high-contrast transmission channeling images of stacking faults in silicon have been produced using a beam of 2 MeV protons focused to a spot size of 60 nm. Over a narrow range of beam tilts to the (011) planes, up to ten periodic intensity oscillations are observed, providing evidence of a long-range coherency of the planar channeled trajectories. This behavior is characterized using Monte Carlo computer simulations, and a phase-space model of planar channeled ion interactions with stacking faults is developed which incorporates all observed channeling and blocking phenomena.

Positively charged, high-energy ions undergo a channeling process when aligned with a crystal direction, in which they are repelled from the lattice plane walls into regions of lower electron density close to the channel center. Channeled ions thus have a smaller probability of scattering from lattice nuclei and a lower rate of energy loss, respectively, producing a dip in the backscattered ion yield and a peak in the energy of ions transmitted through thin crystals [1,2] as a function of beam and crystal alignment.

The use of MeV proton beams, focused to a spot size of $\sim 300$ nm in a nuclear microprobe, was developed to produce spatially resolved transmission channeling images of defects in thinned crystals [3]. A detector on the beam axis records the energy spectrum of the transmitted protons as the beam scans over the sample surface. Planar channeled protons lose energy at typically half the rate of nonchanneled protons [1], and the proportion remaining channeled decreases with depth due to collisions with valence electrons [4]. Any lattice disruption causes additional dechanneling [2]. Transmission channeling images of variations in transmitted energy thus show the distribution of defects such as dislocations, stacking faults [5,6], and precipitates.

Building on phase-space models of planar channeling [7], it was demonstrated that a lattice rotation and translation produce equivalent dechanneling effects [8]. Oscillations were predicted in the transmitted energy of channeled protons versus fault depth. Experimental verification was not possible due to insufficient spatial resolution and small variations in transmitted energy, resulting in low-contrast, "noisy" images.

These limitations have been overcome using a new microprobe which can focus MeV ions to a spot size of 60 nm [9]. The image contrast has been greatly increased using the approach in Fig. 1. This shows the energy spectrum of all 2 MeV protons which are transmitted through a

10 $\mu$m thick [100] silicon sample in (011) alignment, and in a blocked alignment (planar channeling critical angle, $\Psi_p = 0.17°$). In (011) alignment the natural dechanneling half-length is $Z_{1/2} = 3.7 \mu$m [4], so only a small beam fraction remains channeled throughout the crystal. Except for a high-energy channeling tail at planar alignment the spectra are similar, so it is difficult to distinguish small variations in transmitted energy due to additional defect-induced dechanneling [3]. This was overcome by placing a foil in front of the detector. The foil thickness is chosen such that it stops most dechanneled protons, so mainly channeled protons with their higher energy and greater range [1] are recorded. The
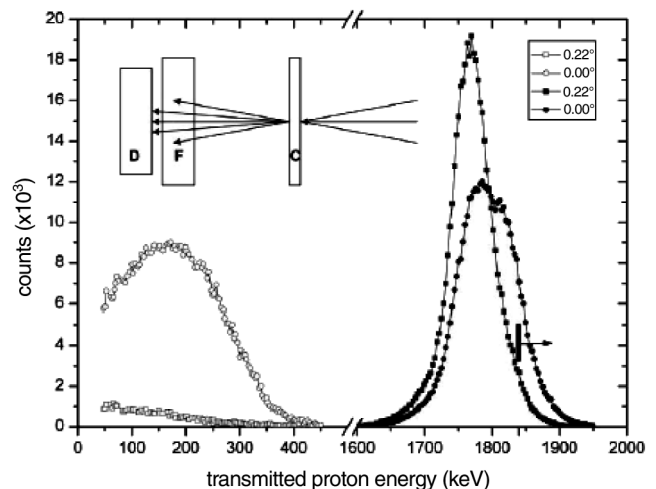


FIG. 1. Energy spectra of all 2 MeV protons which are transmitted through a 10 $\mu$m thick [100] Si crystal (C) into a semiconductor detector (D) on the beam axis (solid symbols). Energy spectra are also shown after the beam passes through a 50 $\mu$m Mylar foil (F) (open symbols). The lower energy threshold of $\sim 1840$ keV which this foil imposes on protons is shown by the arrow.

minimum proton energy which is transmitted through this 50 $\mu$m thick Mylar foil is ~1840 keV, resulting in a factor of 10 difference in the number of protons measured at these alignments. Any defect-induced dechanneling now causes significant contrast variations in the measured proton intensity, as displayed in our transmission channeling results. Since the sole purpose of the foil is to distinguish between channeled and nonchanneled protons, the energy straggle of ~50 keV which it introduces does not matter, and this scheme is simple to implement within the restricted geometry of a high-demagnification microprobe.

The [100] silicon wafer used for analysis contained extrinsic stacking faults, with an average length of 20 $\mu$m, lying on the four inclined {111} planes of the crystal with a translation vector of $\mathbf{R} = \frac{a}{3}\langle 111 \rangle$ normal to the fault plane. The faults are "D-shaped" with the straight edge of each fault meeting the surface along a [011] or [01$\bar{1}$] direction. For transmission channeling analysis this wafer was mechanically thinned and polished to an average thickness of 10 $\mu$m.

Figure 2 shows transmission channeling images of a single fault at different tilts to the (011) planes, recorded with a focused beam convergence angle of ~0.01° ($\ll \Psi_p$). The fault appears dark in Fig. 2(a) because many protons are dechanneled on passing through the fault plane. The additional dechanneling effect of the partial dislocation which bounds the right-hand fault edge is visible as a darker band in the lower right. In Fig. 2(b), the leftmost portion of the fault which is closest to the surface appears as a bright band due to the "blocking to channeling" transition [6]; protons may become channeled at the fault plane due to the lowering of their potential energy. Figure 2(c) shows a smaller region of the central fault portion at a tilt of 0.10°, in which periodic bright and dark bands are visible. The beam dose used during collection of this image was ~$10^{15}$ cm$^{-2}$, considerably below the threshold of
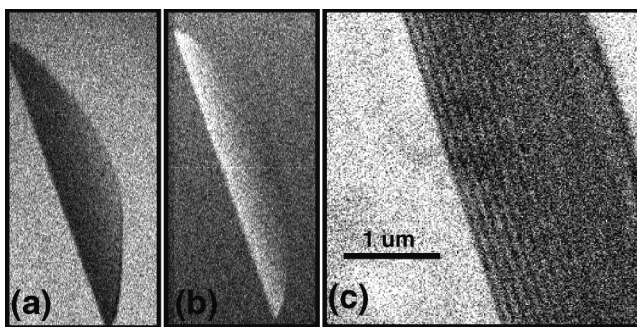
$10^{17}$ cm$^{-2}$ at which MeV proton-induced damage becomes detectable [10].

Figure 3 shows the variation in recorded intensity along a 3.3 $\mu$m horizontal line scan across the center of Fig. 2(c). Each line scan was recorded for 15 min, at a count rate of 3 kHz. For tilts less than 0.05° the fault region is very smooth and no oscillations are observed. At tilts between 0.05° and 0.10°, periodic intensity oscillations are observed, with peak amplitudes decreasing to the right with increasing fault depth. The measured horizontal peak-to-peak distance is $133 \pm 10$ nm, and the angle of inclination of the {111} fault plane to the (001) surface plane is 54.7°. The depth difference at which the peaks occur is thus 133 nm $\times$ tan54.7°, giving a measured wavelength of $\lambda = 185 \pm 14$ nm, compared with calculated values of 230–260 nm and 165 nm for small and large amplitude oscillations [11]. The observed intensity oscillations are thus attributed to protons undergoing large amplitude planar oscillations.

The Monte Carlo channeling code FLUX [12] was used to study the origin of these intensity oscillations. The spatial and angular coordinates and the energy of $1 \times 10^4$ 2 MeV protons which were transmitted through a 10 $\mu$m [100] Si crystal were simulated for different beam tilts to the (011) planes. A lattice translation of $\mathbf{R} =$ 0.65 Å (one-third of the {011} interplanar distance) was introduced to model the effect of the inclined fault plane at depth increments of 40 nm, to a depth of 3.0 $\mu$m. Figure 4(a) shows the variation in transmitted beam intensity versus fault depth. Only those well-channeled protons which are transmitted through the crystal with energy greater than 1840 keV are included, to incorporate the effect of the 50 $\mu$m Mylar foil. These results are



FIG. 2. Transmission channeling images of a stacking fault at tilts of (a) 0.00°, (b) 0.22°, (c) 0.10°. In (a) and (b) the horizontal $\times$ vertical scan area is $4.4 \times 22$ $\mu$m$^2$, and (c) is recorded from a $3.3 \times 3.3$ $\mu$m$^2$ area close to the central fault portion. Regions of low and high recorded intensities appear dark and bright, respectively.
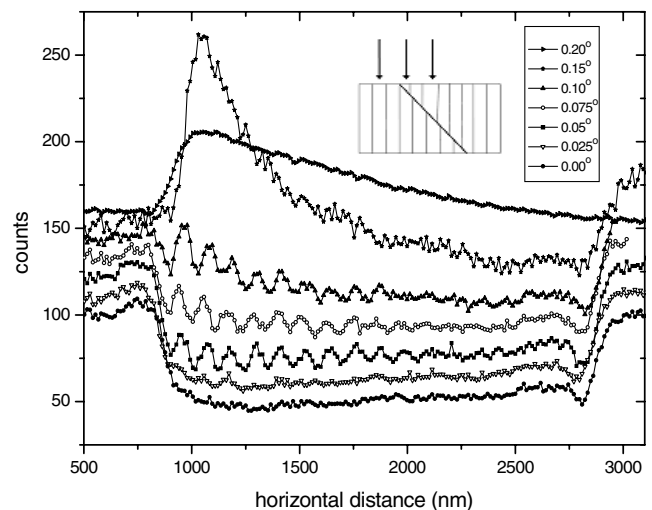


FIG. 3. (a) Horizontal line scans across the center of the fault in Fig. 2(c) for different beam tilts. In each case the number of counts is normalized to 100 from the virgin crystal at the left-hand edge, and offset by an additional 10 counts for clarity. The inset shows the depth of the fault plane increasing to the right.
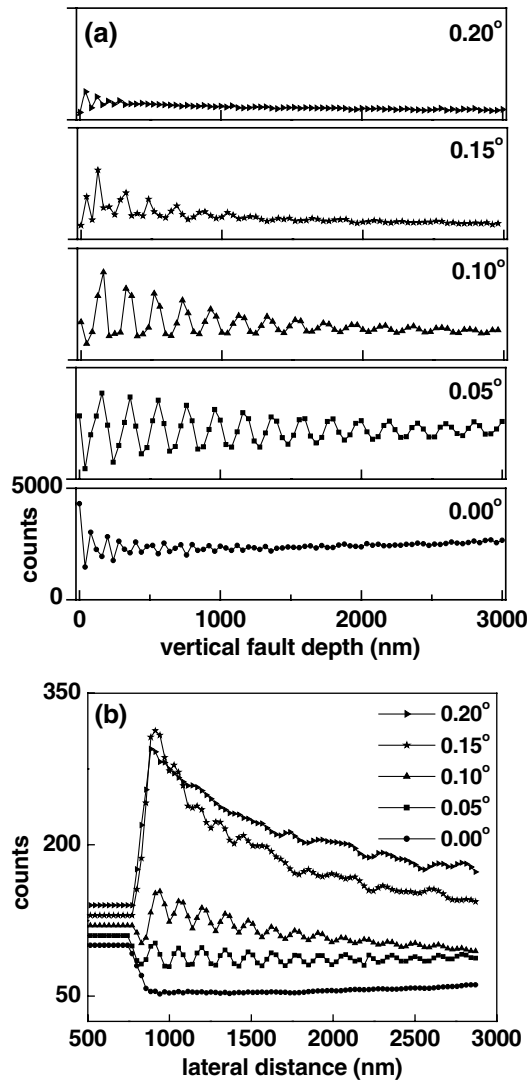
FIG. 4. (a) Simulated transmitted proton intensity versus fault depth, for different beam tilts. Only protons transmitted with energy greater than 1840 keV are included and a zero beam size is assumed. Each box is plotted over the same vertical range of counts. (b) Same simulations convoluted with experimental conditions and displayed in the same format as Fig. 3. A 700 nm region of virgin crystal is incorporated to the left.

plotted in Fig. 4(b) as intensity-versus-horizontal distance across the fault, by multiplying the depth scale by $\tan 54.7°$. Figure 4(b) also incorporates realistic conditions of a beam spot of 60 nm and proton energy straggle through a 50 $\mu$m Mylar foil, instead of a sharp threshold of 1840 keV.

Figure 5 demonstrates the effect of a lattice translation of a stacking fault after the channeled beam has passed through a specific layer thickness. These simulations show the phase-space distributions of protons in which the perpendicular angle $\phi$ to the (011) planes is plotted versus its position with respect to the plane walls. The planar channeled beam occupies an elliptical area which is bounded between the plane walls along the horizontal
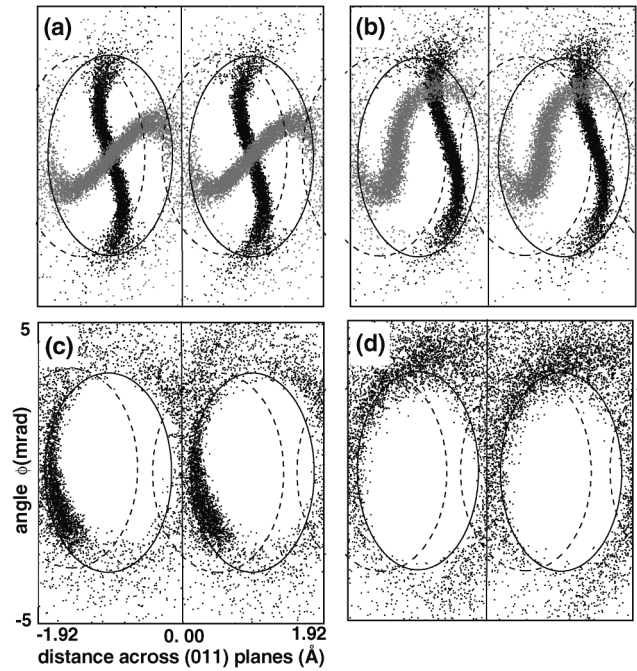


FIG. 5. Phase space plots for beam tilts and layer thicknesses of (a) 0.00°, 40 nm (black symbols) and 80 nm (grey symbols); (b) 0.05°, 40 nm (black) and 160 nm (grey); (c) 0.15°, 120 nm; and (d) 0.20°, 120 nm. The locations of the (011) plane walls and ellipses are shown as solid lines within the layer. When the beam encounters the lattice translation after this layer, the displaced ellipses are shown as dashed lines.

axis, and by $\Psi_p = \pm 3$ mrad along the vertical axis. The channeled beam component rotates clockwise within the ellipses, making one revolution per wavelength depth interval. The lattice translation of the stacking fault after the beam has passed through this layer is incorporated as a horizontal displacement of the ellipses by 0.65 Å.

At planar alignment in Fig. 4(a), small amplitude intensity oscillations are produced for lattice translations close to the surface. The distribution in Fig. 5(a) is symmetric about the ellipse centers at all layer thicknesses. On encountering a lattice translation, some channeled protons will be located outside the displaced ellipses, becoming dechanneled, but a similar number will be located within adjacent ellipses, producing little net effect. The oscillation period is half that at larger tilts, since the phase-space distribution repeats every $\lambda/2$. Oscillations are not resolved in Figs. 3 and 4(b) owing to our finite beam size.

At a tilt of 0.05° in Fig. 5(b), the phase-space distribution is displaced from the ellipse centers and rotates about them. At a layer thickness of 40 nm ($\sim\lambda/4$) the distribution is close to the right edge of the ellipses; on encountering the lattice translation many protons are located outside the displaced ellipses, giving a minima in the transmitted intensity in Fig. 4(a). At a layer thickness of 160 nm ($\sim3\lambda/4$) the distribution is closer to the left edge of the ellipses; on encountering the lattice

translation most protons remain located within the displaced ellipses, giving a maxima in the transmitted intensity.

At a tilt of 0.15° in Fig. 5(c), the beam distribution rotates close to the edge of the ellipses, resulting in large amplitude intensity oscillations in Fig. 4(a). They are not properly resolved in Figs. 3 and 4(b) because of the finite beam spot size, resulting in a continuous region of high counts which appears "noisier" than the other line scans. At a blocking alignment of 0.20° in Fig. 5(d) the beam rapidly occupies all available phase-space regions outside the ellipses. When this distribution encounters a lattice translation at any depth, those protons with $\phi < \Psi_p$, but located outside the ellipses, are projected into the displaced ellipses, becoming channeled. Since the blocked phase-space distribution does not rotate around the ellipses, there are no intensity oscillations, resulting in a continuous distribution of high counts which extends to great depth in Figs. 3 and 4(b).

Datz *et al.* [13,14] studied planar oscillations of high-energy, heavy ions, transmitted through 1 $\mu$m thick gold crystals. In other studies of planar oscillations the beam fraction undergoing coherent oscillations is rapidly masked by the larger decoherent beam. Hence, the nuclear encounter probability versus depth for planar channeled ions is uniform after $3\lambda$ [11,15], and the backscattered intensity of planar channeled helium ions has peaks to depths of $5\lambda$ [16]. Our results provide depth-resolved observations of the transition from coherent planar oscillations to statistical equilibrium, which are observed because the dechanneled beam is stopped by the foil. Intensity peaks are observed over $10\lambda$, evidence that the planar channeled beam is still not in statistical equilibrium even at a depth of $\sim 1.8$ $\mu$m, which is the greatest observed depth for nonequilibrium channeling behavior.

Along with the dechanneling half-length and the oscillation wavelength, we introduce a third parameter to characterize the depth behavior of planar channeled ions. The oscillation amplitude decays exponentially with depth at small tilts, decreasing to half over a "decoherence length" of $\xi \sim 1.1$ $\mu$m. Using $\xi \sim 6\lambda$ and $Z_{1/2} \sim 20\lambda$, we conclude that the {011} channeled beam loses coherency at $\sim 3$ times the rate at which it dechannels. Assuming 70% of protons are channeled at the surface [2], this implies that after passing through a layer thickness of $Z_{1/2}(\approx 3\xi)$, up to 10% still undergo coherent oscillations. This is important for all planar channeling studies of buried layers, where it is assumed that the analysis beam rapidly reaches statistical equilibrium.

We have described ion channeling measurements at a spatial resolution of 60 nm, and demonstrated the use of foil as an energy discriminator to improve the image statistics. Using this facility we have observed long-range coherent planar oscillations, and measured the {011} decoherence length. We note the similarity between the image contrast observed from stacking faults using transmission ion channeling, which may be calculated using Monte Carlo simulations with classical scattering concepts, and that observed using transmission electron microscopy where similar bright and dark fringes are observed and computed by coherent multiple scattering quantum calculations [17].

[1] B. R. Appleton, C. Erginsoy, and W. M. Gibson, Phys. Rev. **161**, 330 (1967).

[2] L. C. Feldman, J. W. Mayer, and S. T. Picraux, *Materials Analysis by Ion Channeling* (Academic Press, New York, 1982).

[3] M. B. H. Breese, D. N. Jamieson, and P. J. C. King, *Materials Analysis using a Nuclear Microprobe* (Wiley, New York, 1996).

[4] L. C. Feldman and B. R. Appleton, Phys. Rev. B **8**, 935 (1973).

[5] P. J. C. King, M. B. H. Breese, P. R. Wilshaw, and G. W. Grime, Phys. Rev. B **51**, 2732 (1995).

[6] P. J. C. King, M. B. H. Breese, P. J. M. Smulders, P. R. Wilshaw, and G. W. Grime, Phys. Rev. Lett. **74**, 411 (1995).

[7] S. T. Picraux, W. R. Allen, R. M. Biefeld, J. A. Ellison, and W. K. Chu, Phys. Rev. Lett. **54**, 2355 (1985).

[8] M. B. H. Breese and P. J. M. Smulders, Phys. Rev. Lett. **81**, 5157 (1998).

[9] F. Watt, J. A. van Kan, I. Rajta, A. A. Bettiol, T. F. Choo, M. B. H. Breese, and T. Osipowicz, Nucl. Instrum. Methods Phys. Res., Sect. B **210**, 14 (2003).

[10] P. J. C. King, Ph.D. dissertation, University of Oxford, 1993.

[11] M. B. H. Breese, P. J. C. King, G. W. Grime, P. J. M. Smulders, L. E. Seiberling, and M. A. Boshart, Phys. Rev. B **53**, 8267 (1996).

[12] P. J. M. Smulders and D. O. Boerma, Nucl. Instrum. Methods Phys. Res., Sect. B **29**, 471 (1987).

[13] S. Datz, C. D. Moak, T. S. Noggle, B. R. Appleton, and H. O. Lutz, Phys. Rev. **179**, 315 (1969).

[14] S. Datz, B. R. Appleton, and C. D. Moak, in *Channeling, Theory, Observation and Applications*, edited by D. V. Morgan (Wiley, London, 1973), Chap. 6.

[15] J. F. Barrett, Phys. Rev. B **3**, 1527 (1971).

[16] F. Abel, G. Amsel, M. Bruneaux, C. Cohen, and A. L'Hoir, Phys. Rev. B **12**, 4617 (1975).

[17] P. B. Hirsch, A. Howie, R. Nicholson, D. W. Pashley, and M. J. Whelan, *Electron Microscopy of Thin Crystals* (Krieger, Malabar, FL, 1977).